Available online at www.sciencedirect.com

jmr&t Journal of Materials Research and Technology

journal homepage: www.elsevier.com/locate/jmrt

Original Article

# Effect of compression temperature on deformation of CaO–CaS–$Al_2O_3$–MgO inclusions in pipeline steel

Yi Wang [a], Lifeng Zhang [b,*], Ying Ren [a,**], Zushu Li [c,***], Carl Slater [c], Kaiyu Peng [a], Fenggang Liu [a], Yanyu Zhao [a]

[a] School of Metallurgical and Ecological Engineering, University of Science and Technology Beijing (USTB), Beijing, 100083, China

[b] State Key Laboratory of Metastable Materials Science and Technology, School of Mechanical Engineering, Yanshan University, Qinhuangdao City, Hebei Province, 066004, China

[c] Advanced Steel Research Centre, WMG, University of Warwick, Coventry, CV4 7AL, UK

ARTICLE INFO

*Article history:*
Received 4 November 2020
Accepted 25 January 2021
Available online 3 February 2021

*Keywords:*
Inclusion deformation
Inclusion transformation
Semi-solid rolling
Pipeline steel
Thermodynamics
Kinetics

ABSTRACT

Plain strain deformation trials were carried out on samples of pipeline steels at 1473 K, 1673 K and 1723 K, respectively. The deformation of inclusions in the solid steel at different temperatures and in the semi-solid steel was studied. The composition of inclusions changed from 60.62%$Al_2O_3$–16.10%CaO–10.27%MgO–13.01%CaS before deformation to 60.59%$Al_2O_3$–13.03%CaO–12.74%MgO–13.63%CaS, 59.69%$Al_2O_3$–7.04%CaO–11.51%MgO–21.76%CaS, and 68.26%$Al_2O_3$–22.56%CaO–6.68%MgO–2.5%CaS with corresponding deforming temperatures of 1473 K, 1673 K and 1723 K. While the average aspect ratio of inclusions increased from 1.28 to 2.23, 1.32, and 1.35, respectively. Thermodynamic calculations performed by FactSage 7.0 verified the composition transformation from CaO to CaS during the solidification and cooling process of the steel. A kinetic model was used to calculate the dynamic transformation of the inclusion composition at compression temperatures. The inclusion transformation ratio from CaO to CaS increased from 38.28% at 1473 K to 50.50% at 1673 K. For the deformation in the solid steel at the temperature below 1673 K, the thickness of the hard phase CaS increased with the soaking temperature, while the hardness of the steel matrix decreased. The larger hardness difference between inclusions and the steel matrix led to a higher aspect ratio of inclusions after deformation. For the deformation in the semi-solid steel, the small difference of hardness between the soft inclusion phase and the soft steel matrix resulted in a low aspect ratio of inclusions in the semi-solid steel after deformation.



* Corresponding author.
** Corresponding author.
*** Corresponding author.
E-mail addresses: zhanglifeng@ysu.edu.cn (L. Zhang), yingren@ustb.edu.cn (Y. Ren), z.li.19@warwick.ac.uk (Z. Li).

https://doi.org/10.1016/j.jmrt.2021.01.107

## 1. Introduction

The existence of non-metallic inclusions in steels is inevitable. Many defects in rolled products are caused by the inclusion deformation. The rolling temperature has a striking effect on the inclusion deformation through properties of inclusions and the steel matrix, such as relative plasticity of inclusions [1,2]. Properties of inclusions, such as hardness, size, distribution, and chemical compositions are key factors of the inclusion deformation. The relationship between the relative plasticity of inclusion and the inclusion hardness has been obtained from the measurement of inclusion and matrix hardness at different temperatures for a number of real and artificial inclusion systems [1]. The relative plasticity of inclusion was related to the ratio of inclusion hardness to steel hardness. Statistical analysis showed that the Young's modulus exhibited a good linear correlation with Vickers hardness at low temperature [3], which was used to evaluate the low-temperature deformability of inclusions. However, there was no relationship between the high-temperature deformation and the low-temperature Young's modulus of inclusions [4]. It was reported that the inclusion deformability increased with inclusion size under certain conditions of temperature and reduction [5]. Finite element simulation on deformation behavior of inclusions in stainless steel strips agreed well with the experimental data, indicating that as the inclusion size increased, the inclusion plasticity gradually increased [6]. The inclusion deformation was also influenced by the inclusion distribution as the stress and thermal field of rolling piece varied with positions. Simulations on the deformation behavior of inclusions in different positions of steel strips showed the deformation of inclusions decreased with an increase in the distance between the inclusion and the strip surface [7]. Deformation properties could be estimated by the inclusion composition. For instance, MnS inclusions were plastically deformable during the hot rolling process in the formation of stringers. On the contrary, $Al_2O_3$ inclusions were broken into pieces under a large reduction. For Si–Mn killed steels, the deformation of inclusions was effectively improved by the lower melting temperature during hot rolling, while the target of inclusions under cold-drawing was $SiO_2$-rich ones with low Young's modulus [4,8]. For small size inclusions in Al-killed Ca-treated steel plates, calcium aluminate inclusions, with low melting temperature, were elongated during the hot rolling process, even if they were covered by a CaS layer, while low modified inclusions were difficult to be deformed. For large size inclusions in Al-killed Ca-treated steel plates, calcium aluminate inclusions were continuously deformed during hot rolling, while inclusions containing CaS and spinel were broken into pieces [9–11]. It is worth mentioning that inclusions transform continuously during the whole process of casting, heating, and rolling [12,13]. The transformation of inclusions during heat treatment has been widely studied in recent years [14–18]. However, the effect of inclusion transformation on inclusion deformation during the rolling process has rarely been investigated.

In the current study, inclusion deformation during plain strain compression of solid steel and semi-solid steel was studied using Gleeble HDS-V40 CC-DR and semi-solid simulator. The effect of compression temperature on inclusion deformation was discussed.

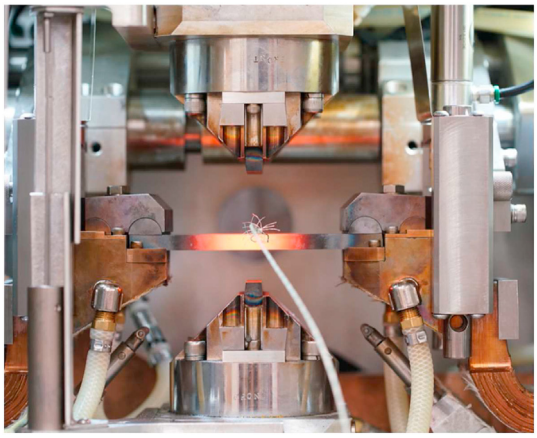

**Fig. 1 – Device layout.**

## 2. Methodology

Steel samples of 160 mm × 10 mm × 25 mm size were cut from the slab of a pipeline steel. Main compositions of the steel are listed in Table 1. Gleeble HDS-V40 thermomechanical simulator was used for direct resistance heating and plain strain compression trials. Three tests were carried out in a vacuum of $5 \times 10^{-3}$ mbar. Thermocouples were connected to the surface of each steel sample at the midpoint of its length. Steel samples were clamped and water cooled at both ends, while the center part was heated to the target temperature under the control of the thermocouple. The layout is shown in Fig. 1.

The experimental scheme is listed in Table 2. Samples were heated to 1473 K, 1673 K, and 1723 K, respectively at the rate of 5 K/s, and held for 2 min before compression, which was followed by a rapid cooling.

The high temperature zone was limited near the midpoint of the sample length. Therefore, small cuboids of metallographic samples were cut from the center of the samples after-deformation, as shown in Fig. 2. Metallographic samples were mounted, ground, and polished. An automated scanning electron microscope was used for inclusion analysis, concentrating on the dash area, which was 3 mm in width and roughly 8 mm along sample thickness, as shown in Fig. 2. The accelerating voltage was 15 kV and the minimum size of detected inclusions was set as 2 μm. The output of element

**Table 1 – Chemical composition of the steel (wt %).**

| C | Si | Mn | P | S | $Al_s$ | Ca | Mg | T.O |
|---|---|---|---|---|---|---|---|---|
| 0.073 | 0.18 | 1.48 | 0.0082 | 0.0014 | 0.021 | 0.0008 | 0.0003 | 0.0019 |

**Table 2 – Experimental scheme.**

| Sample | Temperature (K) | Holding time (s) | Reduction (%) | Strain rate ($s^{-1}$) |
|---|---|---|---|---|
| A-1473 K | 1473 | 120 | 20% | 5 |
| B-1673 K | 1673 | 120 | 20% | 5 |
| C-1723 K | 1723 | 120 | 20% | 5 |

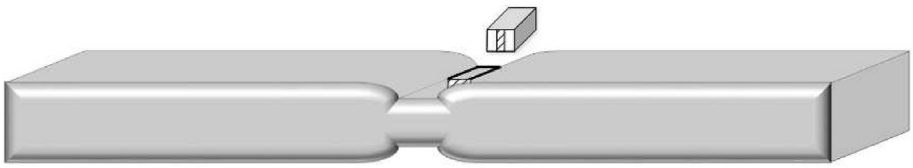

**Fig. 2 – Sampling of metallographic sample.**

contents was transformed into weight percentage of compounds according to the preliminary observation of inclusions. Another metallographic sample was cut from original slab of pipeline steel as the baseline for the comparison of inclusion deformation.

## 3. Inclusions in the steel after deformation

### 3.1. *Deformation of inclusions*

The elemental mapping of a typical inclusion in the original slab is shown in Fig. 3. Inclusions were $Al_2O_3$–MgO–CaO, with a little bit CaS on the surface. Inclusions in the slab were plotted in CaO–CaS–$Al_2O_3$–MgO phase diagrams as shown in Fig. 4. Each dot represented an inclusion. If the CaS content of inclusion was higher than MgO content, it was plotted in the triangle of CaO–CaS–$Al_2O_3$, otherwise in the triangle of CaO–$Al_2O_3$–MgO. The average composition of inclusions in the slab, which was 60.62%$Al_2O_3$–16.10%CaO–10.27% MgO–13.01%CaS, was plot as a red star in Fig. 4. Inclusions were near-spherical before the deformation with an average aspect ratio of 1.28.

The aspect ratio distribution of inclusions in steel samples after deformation is shown in Fig. 5. Each dot represented an inclusion particle. The aspect ratio of each inclusion was denoted by the size of dot. There was no obvious difference along the thickness or width of each steel sample. The size of circles in Fig. 5(a) was larger than (b) and (c), indicating a larger deformation of inclusions at 1473 K. The average aspect ratio of inclusions increased from 1.28 in the original slab to 2.23 in the steel sample deformed at 1473 K, while the average aspect ratios of inclusions were 1.32 and 1.35 in steel samples deformed at 1673 K and 1723 K, respectively.

### 3.2. *Composition of inclusions*

Inclusions were plotted in CaO–CaS–$Al_2O_3$–MgO phase diagrams as shown in Fig. 6. In Fig. 6(a), the average composition of inclusions in the steel sample deformed at 1473 K

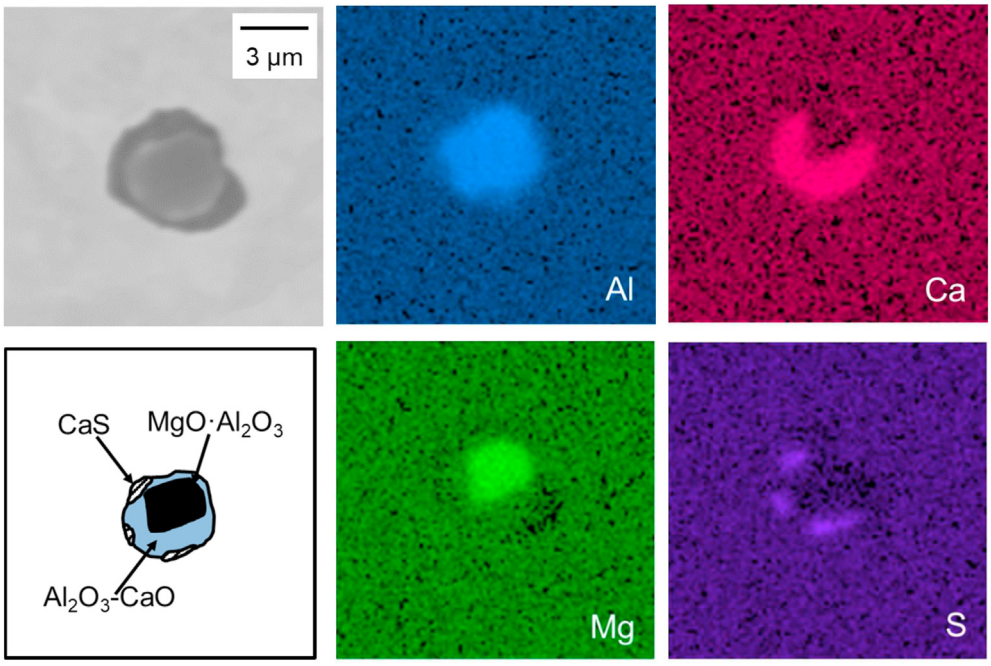


**Fig. 3 – Morphology and elemental mapping of inclusions in the original slab.**

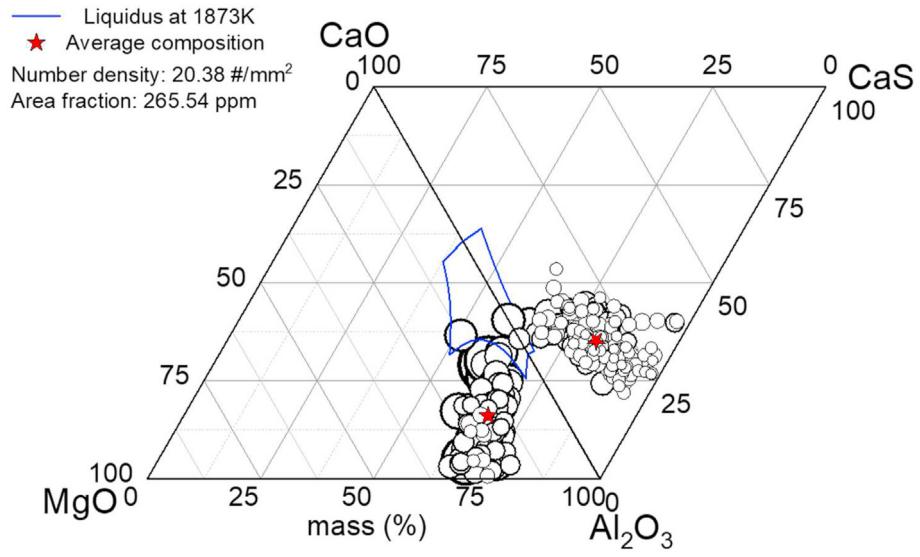


**Fig. 4 – Distribution of inclusion composition in the original slab.**

was 60.59%$Al_2O_3$–13.03%CaO–12.74%MgO–13.63%CaS, which was close to the composition of inclusions in the original slab. The transformation of inclusions from CaO to CaS in the solid steel took place during the heating time of 2 min [17]. The CaS content of inclusions was 0.62% higher, while CaO content decreased by 3.07%. For the steel sample deformed at 1673 K, the red star moved further away from the CaO corner to the CaS corner in the CaO–CaS–$Al_2O_3$–MgO phase diagram as shown in Fig. 6(b). The average composition of inclusions in the steel sample was 59.69% $Al_2O_3$–7.04%CaO–11.51%MgO–21.76%CaS, indicating that the transformation of inclusions from CaO to CaS was promoted by the increase of temperature from 1473 K to 1673 K. In the steel sample deformed at 1723 K, the average composition of inclusions was 68.26%$Al_2O_3$–22.56% CaO–6.68%MgO–2.5%CaS. It implied that the transformation of inclusions at 1723 K was totally different from the ones at 1473 K and 1673 K.

The elemental mapping of typical inclusions in each sample is shown in Fig. 7. Inclusions after deformation were still ellipsoids. There were MgO·$Al_2O_3$ phase, $Al_2O_3$–CaO-(MgO) phase, and various amounts of CaS·phase in inclusions. The CaS outer layer wrapped the oxide core phase. The content of CaS phase in Fig. 7(b) was higher than that in Fig. 7(a), which was almost equal to that in Fig. 3. For Fig. 7(c), there was little CaS content in inclusions in the steel sample deformed at 1723 K. It was consistent with the average compositions shown in Fig. 6.

The number density and average equivalent diameter of inclusions in samples after deformation at 1473 K, 1673 K and 1723 K are shown in Fig. 8. There was not much difference in the number and the size of inclusions among these samples,

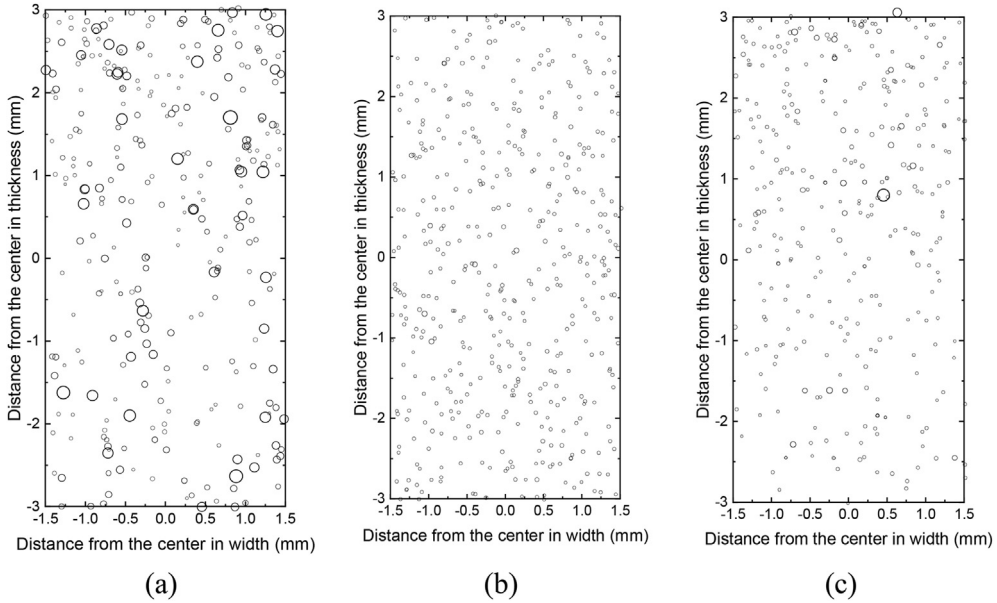


**Fig. 5 – Aspect ratio distribution of inclusions deformed at the temperature of (a) 1473 K, (b) 1673 K, (c) 1723 K.**

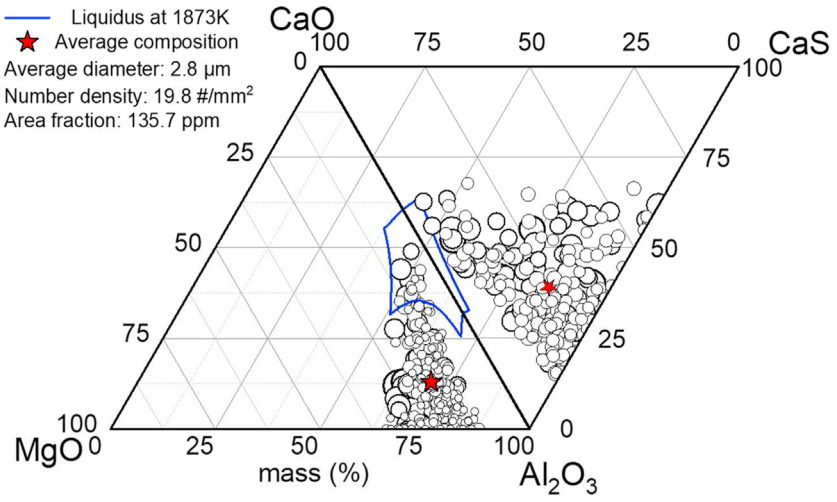


(a)

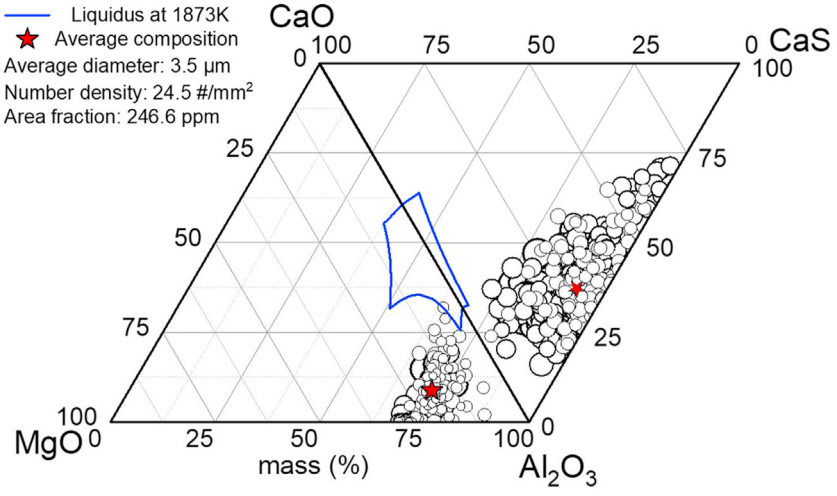


(b)

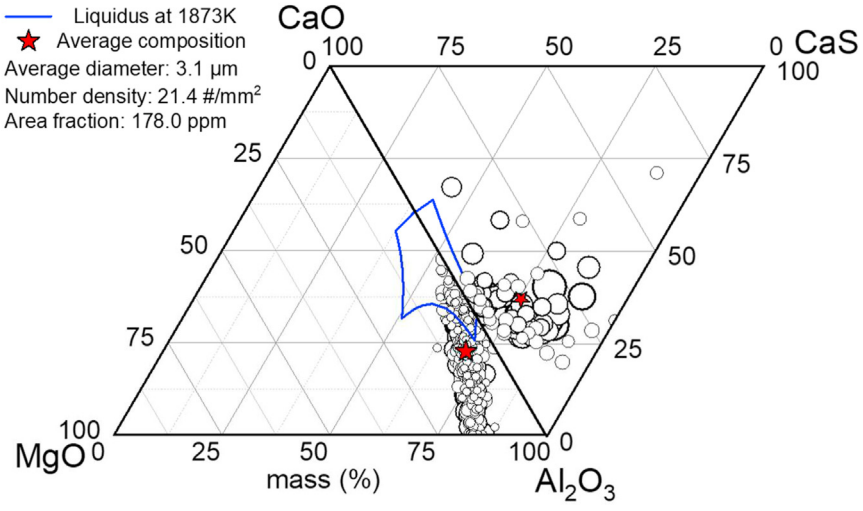


(c)

**Fig. 6 – Distribution of inclusions in steel samples deformed at the temperature of (a) 1473 K, (b) 1673 K, (c) 1723 K.**

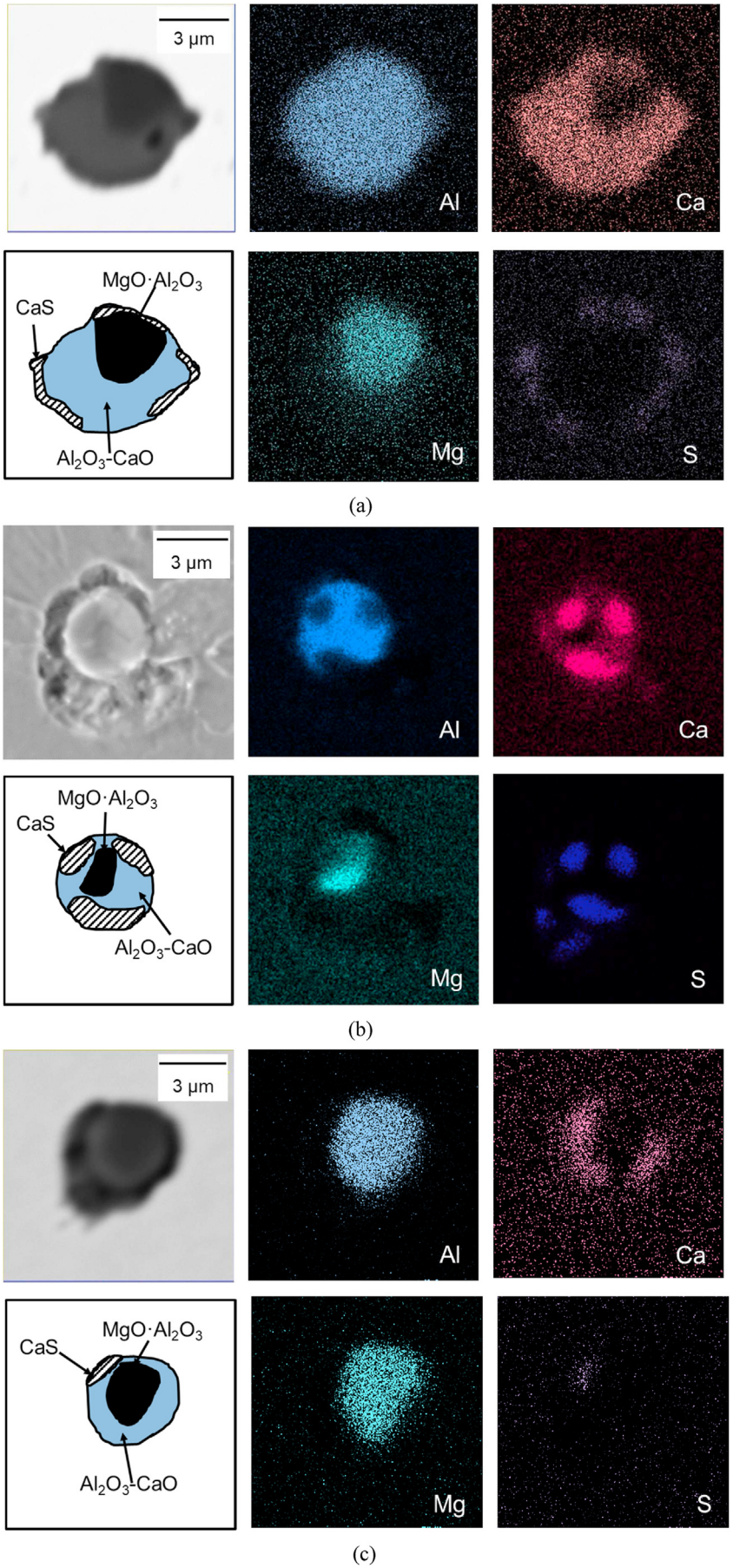


**Fig. 7 – Morphology and elemental mapping of inclusions in samples deformed at the temperature of (a) 1473 K, (b) 1673 K, (c) 1723 K.**

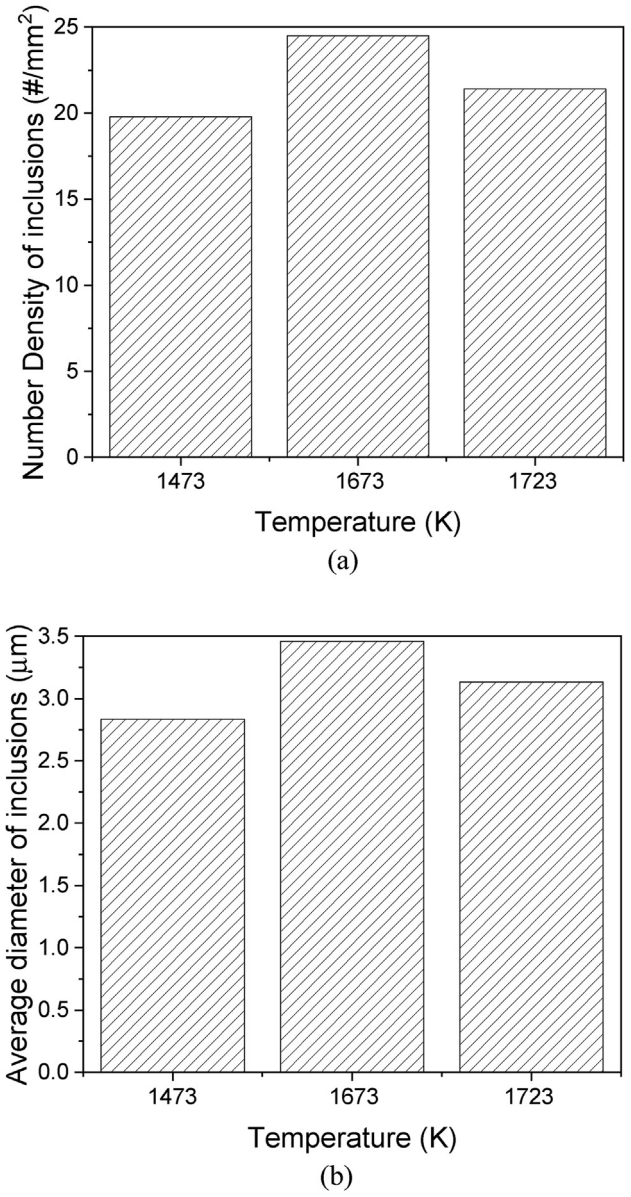


**Fig. 8 – Number density and average diameter of inclusions in samples after deformation. (a) number density, (b) average equivalent diameter.**

indicating that the change of the inclusion composition was mainly caused by the transformation of the original inclusions instead of the precipitation of new inclusions at the soaking temperature. The decrease of average equivalent diameter of inclusions in steel samples deformed at 1473 K was probably due to higher aspect ratio.

### 3.3. *Relationship between the inclusion deformation and the composition transformation*

The variations of inclusion composition and aspect ratio with deformation temperatures are shown in Fig. 9. When the deformation temperature increased from 1473 K to 1673 K, the aspect ratio of inclusions decreased. While for inclusion compositions, the CaS content increased, CaO content decreased, the contents of $Al_2O_3$ and MgO hardly changed. It

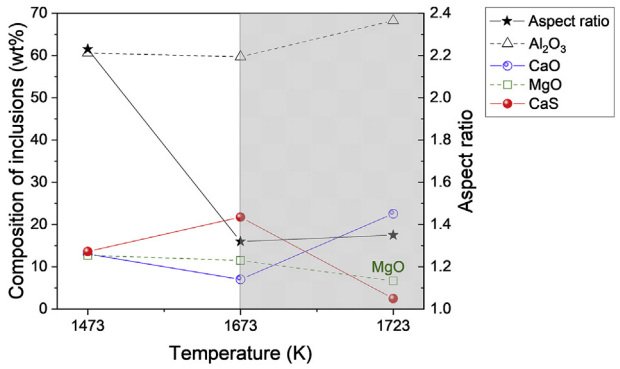


**Fig. 9 – Relationship between the inclusion deformation and the composition transformation.**

implied that the aspect ratio of inclusions decreased with an increase in the transformation ratio from CaO to CaS. However, as the deformation temperature further increased to 1723 K, there was no such relationship between the aspect ratio and the composition change. Though reverse transformation between CaO and CaS was more severe, the aspect ratios of inclusions in steel samples deformed at 1673 K and 1723 K were almost the same.

## 4. Thermodynamics of the inclusion transformation

Thermodynamic calculation of the inclusion transformation was preformed using the thermodynamic software FactSage 7.0 with databases of FactPS, FToxide, and FSstel. The amount of inclusion phases and the composition of inclusions during the solidification and cooling processes of the steel are shown in Fig. 10(a) and (b). Components in Fig. 10(a) were normalized in Fig. 10(b) without consideration of MnS. At the steelmaking temperature, inclusions were liquid calcium aluminate and solid spinel in the molten steel. As the temperature decreased during the solidification of the steel, the liquid phase of inclusion changed to solid phases of $CaO{\cdot}2Al_2O_3$, $MgO{\cdot}Al_2O_3$, and CaS at the temperature between liquidus and solidus of the steel. During further cooling process, $CaO{\cdot}2MgO{\cdot}8Al_2O_3$ and CaS phases precipitated, while the amount of $MgO{\cdot}Al_2O_3$ phase decreased. Inclusions changed from $Al_2O_3$–CaO–MgO to $Al_2O_3$–CaS–CaO–MgO. The equilibrium compositions of inclusions at 1473 K, 1673 K, and 1723 K were 65.06% $Al_2O_3$–3.80%CaO–9.22%MgO–21.91%CaS, 65.05%$Al_2O_3$–3.80% CaO–9.24%MgO–21.92%CaS, and 64.79%$Al_2O_3$–10.86% CaO–9.90%MgO–14.46%CaS, respectively. The equilibrium compositions of inclusions at 1473 K and 1673 K were almost the same, since the inclusion composition was nearly constant under 1704 K. Only the equilibrium composition of inclusions at 1673 K agreed with the detected values. There was quite a difference between the measured and calculated compositions since the equilibrium was hardly reached during experiments in the current study.

It should be noticed that the actual temperature in the center of the sample was higher than the value detected by the thermocouple, which was connected to the surface of the steel sample. Shrinkage cavities, which indicated the

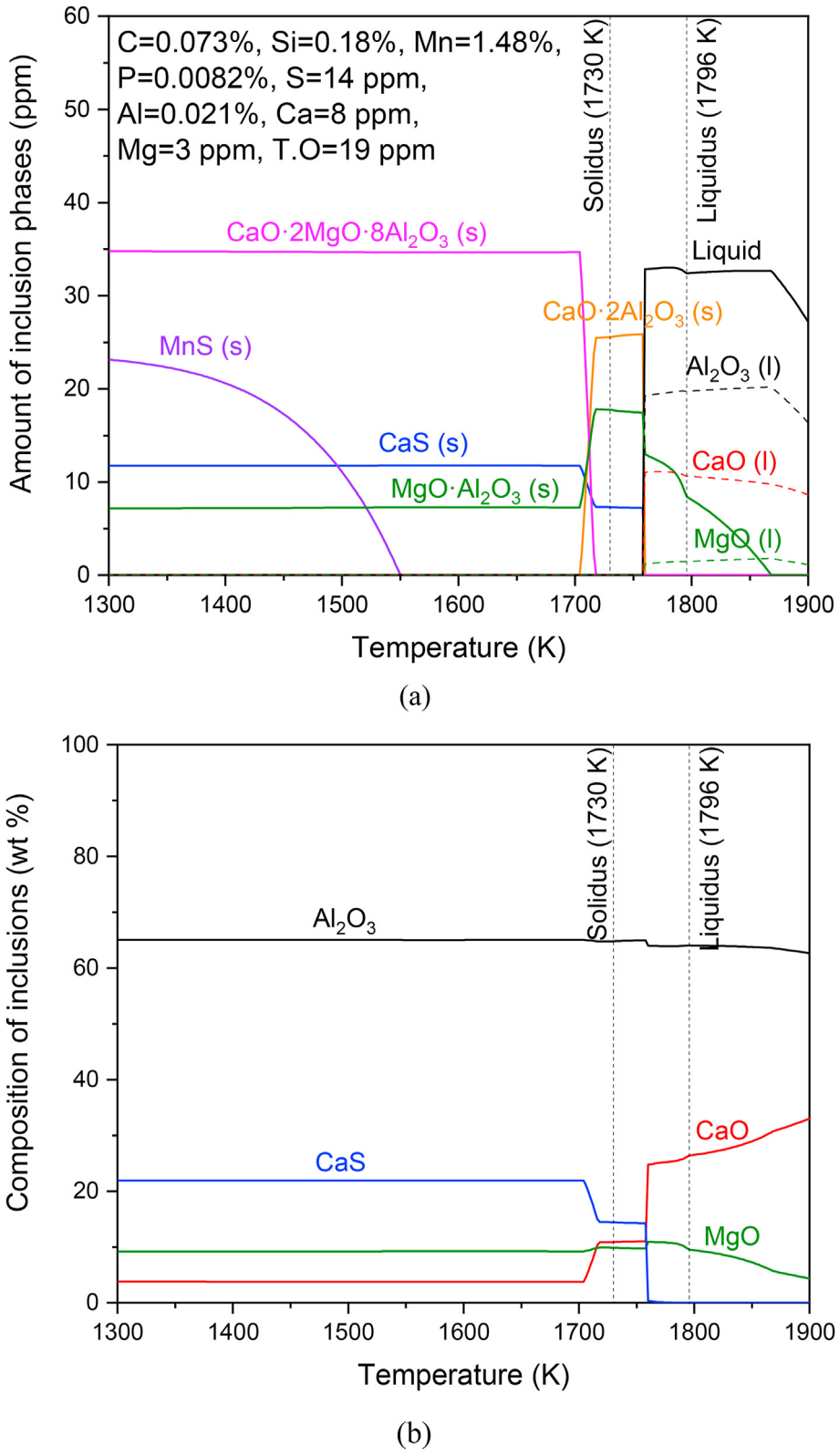


**Fig. 10 – Inclusion transformation during solidification and cooling process of the steel as a function of temperature(a) phase, (b) composition.**

formation of a semi-solid zone, were observed in the center of the steel sample heated up to 1723 K without deformation. Moreover, based on the thermodynamic calculation, the CaS phase precipitated in inclusions at the temperature under 1760 K. Therefore, for the deformation experiment at 1723 K, the actual temperature in the center of the sample was between 1760 K and liquidus (1796 K). The equilibrium composition at 1760 K in Fig. 10 was 64.01%$Al_2O_3$–24.75%

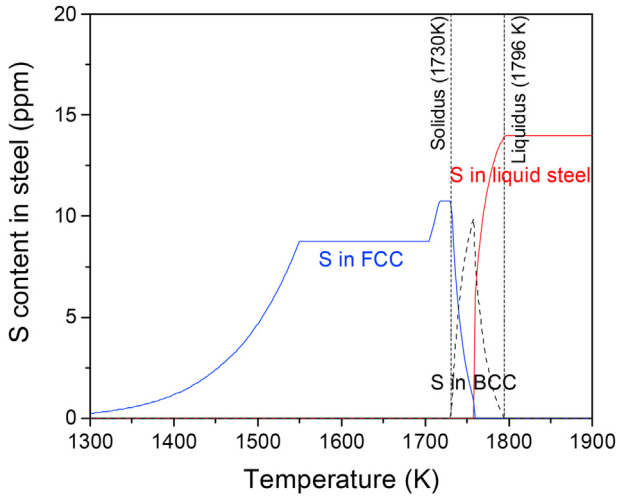


**Fig. 11 – Equilibrated sulfur content in steel matrix.**

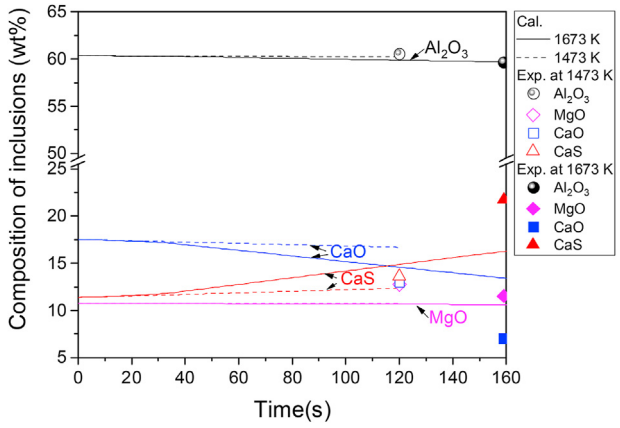


**Fig. 12 – Variation of inclusion composition with time.**

CaO–10.88%MgO–0.36%CaS, which was close to the detected value of 68.26%$Al_2O_3$–22.56%CaO–6.68%MgO–2.5%CaS. Calcium aluminate inclusions are much softer than the inclusions of MgO·$Al_2O_3$ wrapped by a thick hard shell of CaS phase. Better deformation performances and lower crack incidence will be exhibited in the following sequence of hot or cold rolling process at a lower temperature [19].

## 5. Kinetics of the inclusion transformation

A kinetic model of inclusion transformation during the solidification and cooling processes was developed to calculate the dynamic transformation of inclusion compositions at 1473 K and 1673 K. The transformation of inclusions in the sample deformed at 1723 K was not calculated due to the formation of semi-solid zone and inaccuracy of the temperature. It was assumed that the rate of inclusion transformation was controlled by the element diffusion between the steel matrix and inclusions, and local equilibrium was achieved at the steel–inclusion interface. The main reaction between inclusions and the steel matrix is presented by Eq. (1). The diffusion rate of Al, Mg, Ca, S, and O is shown by Eq. (2).

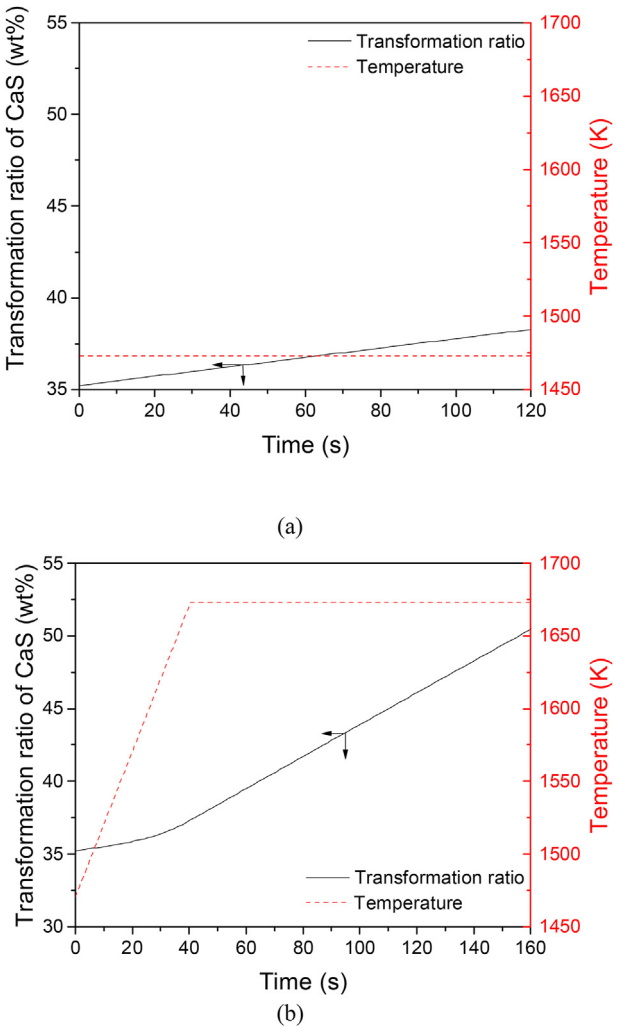


**Fig. 13 – Variation of transformation ratio of CaS in inclusions with time (a) 1473 K, (b) 1673 K.**

Details of the kinetic model is presented in a previous study [20].

$$3x(Al_2O_3) + 3y(CaO) + 2(y-z)[Al] + 3z[Mg] + 3y[S] = (3x+y-z)(Al_2O_3) + 3z(MgO) + 3y(CaS) \quad (1)$$

$$\frac{dm}{dt} = \frac{[\%i]_{bulk} - [\%i]_{int}}{100} 4\pi D r \rho_{steel} \quad (2)$$

where [%i] is the mass percentage of element; D is the diffusivity, $m^2/s$; r is the radius of the inclusion, m; and $\rho_{steel}$ is the density of the steel matrix, $kg/m^3$.

The equilibrated sulfur content in the steel matrix at various temperatures calculated by FactSage 7.0 is shown in Fig. 11. The sulfur content in the steel matrix was below 3.33 ppm when the temperature was under 1473 K. Therefore, the heating process under 1473 K was neglected in the kinetic calculation. For the sample deformed at 1473 K, the total time of the inclusion transformation was 120 s. The total time for the sample deformed at 1673 K was the sum of time for the temperature increased from 1473 K to 1673 K at a rate of 5 K/s and the holding time of 120 s at 1673 K.

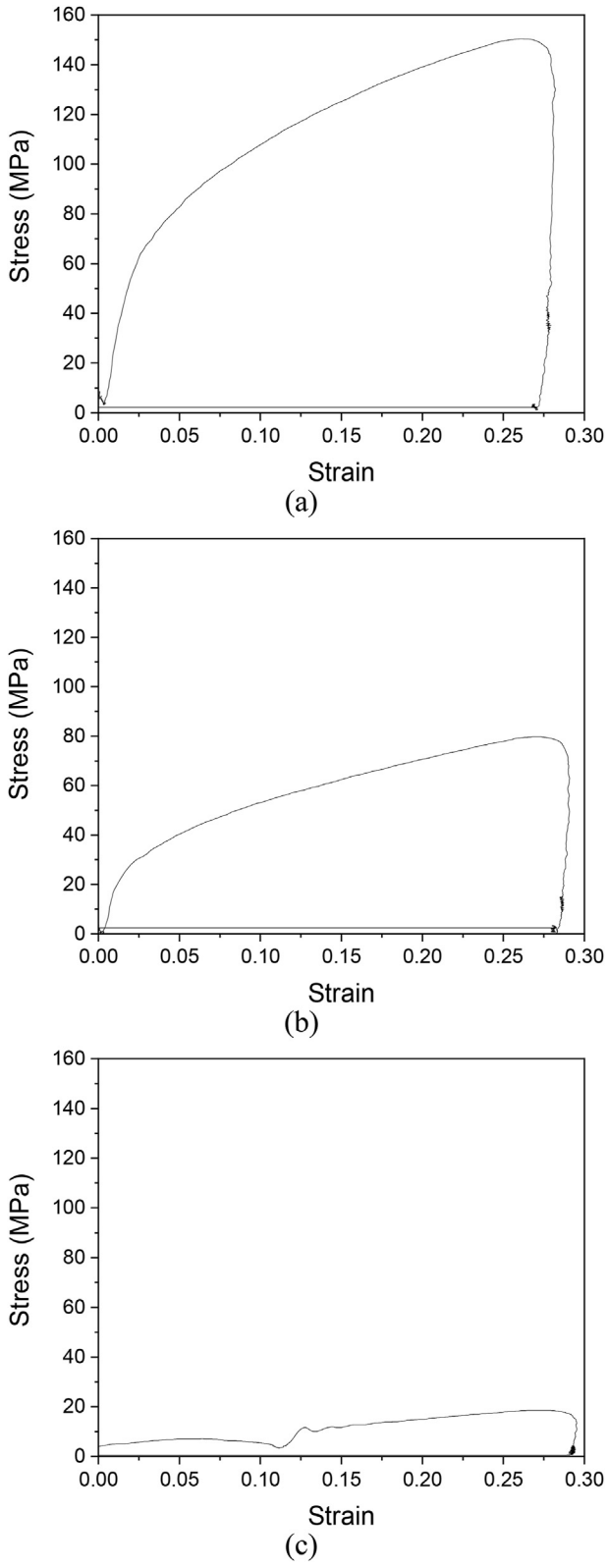


**Fig. 14 – Stress–strain curves during deformation at (a) 1473 K, (b) 1673 K, (c) 1723 K.**

The variation of inclusion composition with time in steel samples deformed at 1673 K and 1473 K was calculated, as shown in Fig. 12 by solid and dash lines. At both 1473 K and 1673 K, the CaO content of inclusions decreased with time, while the CaS content changed inversely. Contents of $Al_2O_3$ and MgO in inclusions changed slightly. However, the transformation rate from CaO to CaS at 1673 K was much faster than that at 1473 K, especially after the temperature at sample surface reaching 1673 K. The calculated composition of inclusions was 60.23%$Al_2O_3$–16.70%CaO–10.71%MgO–12.36% CaS after holding at 1473 K for 120 s, while it was 59.69% $Al_2O_3$–13.39%CaO–10.62%MgO–16.31%CaS after the temperature was increased to 1673 K and held for 120 s. The detected average composition of inclusions was plotted in Fig. 12 as scatters with different colors and shapes. It was noted that the detected content of CaS in inclusions was a little bit higher than the calculated result at 1673 K, while CaO content was lower. It was probably because the actual temperatures in the middle of steel samples were higher than the values detected by the thermocouple connected to the surface. Generally, the composition of inclusions agreed well between kinetic calculated results and detected values.

Fig. 13 shows the variation of the transformation ratio of CaS in inclusions with time in steel samples deformed at 1473 K and 1673 K. Transformation from CaO to CaS was completed by 38.28% after soaking at 1473 K for 120 s. It increased to 50.50% at 120 s after the temperature was increased to 1673 K.

## 6. Mechanism of the inclusion deformation

The aspect ratio of inclusions after deformation was decided by strain partitioning, which was caused by the difference of hardness between the inclusion phase and the steel phase [1,21]. For the hardness of the steel matrix, the stress–strain curves during the plain strain deformations are shown in Fig. 14. The stress under the same strain decreased with an increase in soaking temperature, indicating that steel samples got softer under higher heating temperature during the deformation.

Inclusions consisted of $MgO{\cdot}Al_2O_3$ phase, $Al_2O_3$–CaO-(MgO) phase, and CaS·phase. The melting point of $MgO{\cdot}Al_2O_3$ is 2523 K, while it is 2673 K for CaS. The melting point of calcium aluminates was calculated using FactSage 7.0 based on the detected inclusion composition. It showed that the melting point of calcium aluminate phase in the steel sample deformed at 1673 K was 117 K higher than that in the steel sample deformed at 1473 K, but much lower than those of $MgO{\cdot}Al_2O_3$ phase and CaS phase. Generally, inclusion phases with higher melting points tend to exhibit higher hardness [22]. Therefore, combined with the difference of CaS layer thickness and the hardness of the steel matrix, the difference in the amount of deformation of inclusions in steel samples is proposed in Fig. 15.

The summation of the strains of the inclusion phase and the steel matrix, represented by the shaded area in the lower part of Fig. 15, were equal among samples deformed at different temperature under the same condition of reduction. In the current study, the hardness of the steel matrix decreased with increasing temperature. The size and the $MgO{\cdot}Al_2O_3$ content of inclusions were similar among samples. When steel samples were deformed in the solid state, the

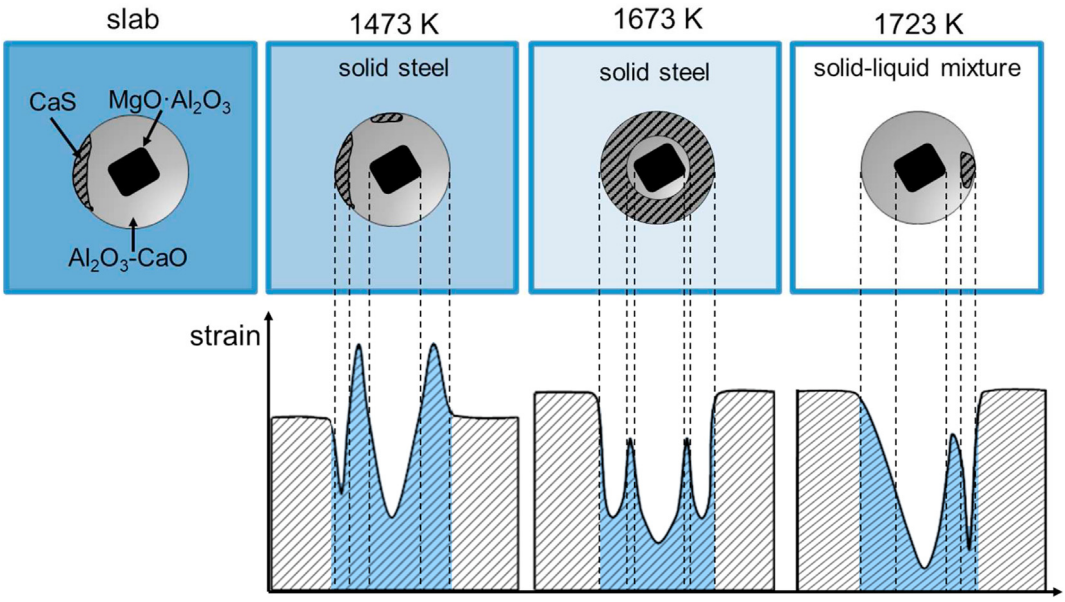


**Fig. 15 – Deformation mechanism of inclusions in the steel.**

thickness of hard CaS outer layer increased with temperature due to the higher equilibrium content of sulfur and diffusion rate of elements. Therefore, the difference between the steel phase and the inclusion phase was larger in steel sample deformed at 1673 K than that deformed at 1473 K due to the harder inclusion phase and softer steel phase at 1673 K. More strain concentrated on the soft phase than the hard phase [23]. The total strain of the inclusion phase, which was the sum of $MgO{\cdot}Al_2O_3$ phase, $Al_2O_3$–CaO–(MgO) phase, and CaS·phase, decreased with temperature, shown by dark color in the lower part of Fig. 15. For the deformation in the semi-solid steel, although the calcium aluminate inclusion phase was softer than those in the other two solid samples, the hardness of semi-solid steel phase was also much lower. The small difference of hardness between the soft inclusion phase and the soft steel matrix resulted in a low aspect ratio of inclusions in semi-solid steel after deformation. Due to the small reduction of 20%, high temperatures during compression and the temperature control mechanism of the operation system, the influence of the deformation on transformations of inclusion composition and steel phase was neglectable.

## 7. Conclusions

In the current study, deformation of inclusions in the solid pipeline steel at 1473 K, 1673 K, as well as in the semi-solid steel were studied by experiments, thermodynamic analysis, and kinetic calculation. The following conclusions were derived:

(1) Inclusions were $Al_2O_3$–MgO–CaO–CaS in the original slab with an average aspect ratio of 1.28. After deformation, the average aspect ratio of inclusions increased to 2.23, 1.32 and 1.35 in steel samples deformed at 1473 K, 1673 K and 1723 K respectively.

(2) The CaO in inclusions transformed into CaS in solid steel samples between 1473 K and 1673 K. The transformation rate of inclusions increased with temperature due to an increase in the thermodynamic equilibrium content of sulfur and diffusion rate of elements at higher temperatures. Inclusions in the steel sample deformed at a detected surface temperature of 1723 K was $Al_2O_3$–CaO–(MgO) with little CaS, since the thermodynamic calculated results showed that CaS can hardly formed in the liquid steel.

(3) For the deformation in the solid steel at the temperature below 1673 K, the thickness of the precipitated hard phase CaS increased with temperature, while the hardness of the steel matrix decreased. The larger hardness difference between inclusions and the steel matrix led to a higher aspect ratio of inclusions after deformation. For the deformation in the semi-solid steel, the hardness difference between the soft inclusion phase and the soft steel matrix was small, which resulted in a low inclusion aspect ratio.

## Declaration of Competing Interest

The authors declare that they have no known competing financial interests or personal relationships that could have appeared to influence the work reported in this paper.

## Acknowledgements

The authors are grateful for support from the National Natural Science Foundation of China (Grant No. U1860206, No. 51725402), S&T Program of Hebei (Grant No.20311004D, 20311005D, 20311006D, 20591001D), the High Steel Center

(HSC) at Yanshan University, Hebei Innovation Center of the Development and Application of High Quality Steel Materials, Hebei International Research Center of Advanced and Intelligent Manufacturing of High Quality Steel Materials.

## REFERENCES

[1] Baker T, Gave K, Charles J. Inclusion deformation and toughness anisotropy in hot-rolled steels. Met Technol 1976;3(1):183–93.
[2] Luo C, Ståhlberg U. Deformation of inclusions during hot rolling of steels. J Mater Process Technol 2001;114(1):87–97.
[3] Jiang X, Zhao J, Jiang X. Correlation between hardness and elastic moduli of the covalent crystals. Comput Mater Sci 2011;50(7):2287–90.
[4] Zhang L, Guo C, Yang W, Ren Y, Ling H. Deformability of oxide inclusions in tire cord steels. Metall Mater Trans B 2018;49(2):803–11.
[5] Segal A, Charles J. Influence of particle size on deformation characteristics of manganese sulphide inclusions in steel. Met Technol 1977;4(1):177–82.
[6] Yu H, Liu X, Bi H, Chen L. Deformation behavior of inclusions in stainless steel strips during multi-pass cold rolling. J Mater Process Technol 2009;209(1):455–61.
[7] Yu H, Bi H, Liu X, Chen L, Dong N. Behavior of inclusions with weak adhesion to strip matrix during rolling using FEM. J Mater Process Technol 2009;209(9):4274–80.
[8] Yang W, Guo C, Zhang L, Ling H, Li C. Evolution of oxide inclusions in Si-Mn killed steels during hot-rolling process. Metall Mater Trans B 2017;48(5):2717–30.
[9] Zhao D, Li H, Bao C, Yang J. Inclusion evolution during modification of alumina inclusions by calcium in liquid steel and deformation during hot rolling process. ISIJ Int 2015;55(10):2115–24.
[10] Guo J, Cheng S, Cheng Z, Xin L. Thermodynamics for precipitation of CaS bearing inclusion and their deformation during rolling process for Al-killed Ca-treated steel. Steel Res Int 2013;84(6):545–53.
[11] Guo J, Cheng S, Cheng Z. Mechanism of non-metallic inclusion formation and modification and their deformation during compact strip production (CSP) process for aluminum-killed steel. ISIJ Int 2013;53(12):2142–51.
[12] Holappa L, Hämäläinen M, Liukkonen M, Lind M. Thermodynamic examination of inclusion modification and precipitation from calcium treatment to solidified steel. Ironmak Steelmak 2003;30(2):111–5.
[13] Choudhary S. Thermodynamic evaluation of inclusion formation during cooling and solidification of low carbon Si-Mn killed steel. Mater Manuf Process 2012;27(9):925–9.
[14] Takahashi I, Sakae T, Yoshida T. Changes of the nonmetallic inclusion by heating. Tetsu-To-Hagane 1967;53(3):350–7.
[15] Ren Y, Zhang L, Pistorius C. Transformation of oxide inclusions in type 304 stainless steels during heat treatment. Metall Mater Trans B 2017;48(5):2281–92.
[16] Cheng G, Li W, Zhang X, Zhang L. Transformation of inclusions in solid GCr15 bearing steels during heat treatment. Metals 2019;9(6):642.
[17] Chu Y, Li W, Ren Y, Zhang L. Transformation of inclusions in linepipe steels during heat treatment. Metall Mater Trans B 2019;50(4):2047–62.
[18] Li M, Matsuura H, Tsukihashi F. Effect of Mg-bearing oxide(+TiN) inclusion on microstructure of Fe-16 mass pct Cr ferritic alloy and its evolution during heating at 1573 K (1300 °C). Metall Mater Trans B 2019;50(4):1814–21.
[19] Ervasti E, Ståhlberg U. Void initiation close to a macro-inclusion during single pass reductions in the hot rolling of steel slabs: a numerical study. J Mater Process Technol 2005;170(1–2):142–50.
[20] Ren Q, Zhang Y, Zhang L, Wang J, Ren Y. Prediction on the spatial distribution of the composition of inclusions in a heavy rail steel continuous casting bloom. J Mater Res Technol 2020;9(3):5648–65.
[21] Gove K, Charles J. Further aspects of inclusion deformation. Met Technol 1974;1(1):425–31.
[22] Ladutkin D, Korte E, Bleymehl M, Bruch C, Doppler K. Advantages of Si deoxidation of bearing steels for steel cleanness and for composition and morphology of nonmetallic inclusions in rolled product. Bear Steel Technol 2017;11(1):48–62.
[23] Elango C, Yu S, Naoya K, Goro M, Tadashi F. Effect of ferrite/martensite phase size on tensile behavior of dual-phase steels with nano-precipitation of vanadium carbides. Metall Mater Trans 2019;50(9):4111–26.